Regularities in calculated photoionization cross sections for the halogens

F. Robicheaux and Chris H. Greene
Department of Physics and The Joint Institute for Laboratory Astrophysics, University of Colorado, Boulder, Colorado 80309-0440
(Received 27 March 1992)

The total photoionization cross sections of F, Cl, Br, and I are calculated near the ns^2np^4 thresholds. They show excellent agreement with experiment for all of the halogens except I whose cross section is only in fair agreement with experiment. At the ^1S threshold of Cl our results agree with experiment and with the highest of the previous calculations. These results suggest that atomic theory is now capable of reproducing the dynamics of all the open p-shell atoms with $Z < 54$, at energies near the lower ionization thresholds. We identify a type of mixing which goes beyond the usual recoupling frame transformation and is not present in alkaline-earth atoms, nor in rare-gas atoms.

PACS number(s): 32.80.Fb, 32.80.Dz, 31.20.Di

I. INTRODUCTION

There have been a growing number of experiments [1–4] and calculations [5–8] involving the photoionization of neutral halogens. These species prove to be of great interest due to their similarity to the noble-gas atoms. They challenge theory due to their open outer p shell but the calculations should remain tractable because there is only one electron missing from the outermost shell. However, previous theoretical studies have not achieved the level of accuracy which seems possible with the current state of the art. In fact, only Cl has been theoretically attempted near the lower thresholds with the sophistication necessary for a reasonable description of the spectra. Even with this qualification, there is disagreement between several of the previous calculations just above the $3s^23p^4(^1S_0)$ threshold in Cl [8(a)]. The theoretical understanding of the halogen atoms is not satisfactory compared to that of the rare-gas atoms where very different computational techniques agree with each other and with experiment [9,10]. The Br spectrum is remarkably similar to the Cl spectrum and the I spectrum itself resembles the Br spectrum. These similarities in the experimental spectra must indicate similarities in the atomic dynamics.

In this paper, we describe a series of comparatively-small-scale calculations which accurately reproduce the experimental spectra of F, Cl, Br, and I near the ns^2np^4 ionic thresholds. This region contains prominent autoionizing structures due to the comparable magnitude of the amplitudes for excitation into open and closed channels. We plan to address another interesting energy range, below the $nsnp^5$ thresholds, in subsequent work. We utilize the eigenchannel R-matrix approach [11] (which differs from the Wigner-Eisenbud R-matrix approach [12] in technical details) for the brute force part of the calculation and the multichannel quantum-defect theory (MQDT) to extend the wave functions to distances larger than the R-matrix box radius [13]. The R-matrix calculation is completely nonrelativistic; the wave function is LS coupled in the numerical portion of the calculation with relativistic (spin-orbit) effects incorporated in the MQDT part of the calculation by applying the LS-to-jj frame transformation [10,13]. It has been found necessary to go beyond this standard recoupling frame transformation to account also for the *mixing* of different LS-coupled *core* states which have the same total angular momentum, J_c.

II. STANDARD METHODS

Most of the techniques adopted here to describe photoionization of the halogens are the same as those used for the previous description of the alkaline earths (Be, Mg, Ca, . . .) [14], their negative ions [15], and atomic silicon [16]. We will give a brief description of these techniques, referring the reader to previous literature for more details [14–16]. The following section describes some new features of the code which the extra electrons force us to use. These new features reflect the change in physical description from atoms with a few valence electrons to those with a few holes.

A. Eigenchannel R-matrix approach

The major numerical approximation which we use for the description of the dynamics is the eigenchannel R-matrix procedure [11]. This tool uses a superposition of orthonormal basis functions in a small region of space (called the R-matrix volume) to obtain a variational estimate of the logarithmic derivative of the wave function at a given energy. We define the R-matrix volume by $r_i \le r_c$ (i.e., all electrons confined to radii less than r_c) with r_c being 9 a.u. for all calculations reported here. In particular, the relevant matrix equation for the coefficients of the basis functions, $\psi_{E\beta}=\sum_i y_i(\mathbf{r})C_{i\beta}(E)$, is

$$\underline{\Gamma}\mathbf{C}_\beta = b_\beta \underline{\Lambda}\mathbf{C}_\beta \,, \tag{1}$$

where $\Gamma_{ij}=2\langle y_i|(E-H)|y_j\rangle - \langle\langle y_i|\partial/\partial n|y_j\rangle\rangle$ and $\Lambda_{ij}=\langle\langle y_i|y_j\rangle\rangle$; the double bra-ket notation indicates integration only over the surface of the R-matrix volume [14]. The normal derivative of $\psi_{E\beta}$ is $\partial\psi_{E\beta}/\partial n = -b_\beta\psi_{E\beta}$.

We use the streamlined formulation [16] of the eigen-

channel R-matrix approach which divides the basis set into open functions (where only one of the electron orbitals of the many-electron basis function is nonzero at the R-matrix boundary) and closed functions (where all of the electron orbitals are zero at the boundary). We use only one open (one-electron) orbital for each l due to the numerical difficulties of Gram-Schmidt orthogonalizing two open orbitals with each other and with the closed orbitals. Multielectron matrix elements are much easier to evaluate when all of the different orbitals are orthogonal to each other. We include basis functions representing strong correlations (e.g., $nsnp^6$, $ns^2np^2nd^3$, etc.) as well as scattering-type basis functions (e.g., ns^2np^4md, ns^2np^4ms, etc.) in the closed portion of our basis set. On the whole, the correlation-type basis functions seem to play a smaller role in the halogen dynamics than they do in the dynamics of the alkaline earths. One exception is the F $2s2p^6$ resonance between the ^1D and ^1S ionization thresholds.

B. The approximate Hamiltonian

The major physical approximation concerns the Hamiltonian H which does *not* refer to the full atomic system [14–16]. H is strictly nonrelativistic, not even containing $\mathbf{l}_i\cdot\mathbf{s}_i$ interactions. Most importantly, H only represents the Hamiltonian of the valence shells. The effect of the $Z-7$ inner-core electrons is approximated by a screened Coulomb potential plus a polarization potential. This necessary simplification works well as long as the energy of the full atomic system is smaller than the energy needed to excite an inner-core electron. We feel this approximation is necessary due to the difficulty in describing the dynamics of the inner-core electrons for large Z to sufficient accuracy using standard independent-electron models. The interesting part of the dynamics resulting from the interaction between the valence electrons should not be obscured by inaccuracies in the description of the relatively inert inner core. Also, d- and f-type electrons are especially sensitive to errors in the description of the inner-core electrons which will make this approximation absolutely crucial for the description of the transition metals, our long-term goal. Previous experience with calculations in the alkaline-earth atoms has shown that such use of model potentials to represent the core electrons greatly enhances both the accuracy and efficiency of the computations [16].

The valence electron Hamiltonian in atomic units is

$$H=\sum_i H_V(\mathbf{p}_i,\mathbf{r}_i)+\sum_{\substack{i,j\\ i<j}} 1/r_{ij} -2\sum_{\substack{i,j\\ i<j}} P_1(\cos\theta_{ij})[V_{\rm pol}(r_i)V_{\rm pol}(r_j)]^{1/2}\ , \tag{2}$$

where $\cos\theta_{ij}=\mathbf{r}_i\cdot\mathbf{r}_j/r_ir_j$. The one-electron Hamiltonian contains the interaction of the valence electron with the nucleus and the inner-core electrons and has the form

$$\begin{aligned} H_V(\mathbf{p},\mathbf{r})&=p^2/2+V\\ &=p^2/2-(7+\{Z-7\}\exp\{-\alpha_1^l r\}\\ &\quad+\alpha_2^l r\exp\{-\alpha_3^l r\})/r+V_{\rm pol}(r)\ . \end{aligned} \tag{3}$$

Here $V_{\rm pol}=-\alpha_d[1-\exp\{-(r/r_c)^3\}]^2/2r^4$ represents the interaction of an outer electron with the inner core due to its polarizability. The l dependence of α_i^l causes V to be a nonlocal potential. We use the values of Ref. [17] for the dipole polarizability, α_d, of the inner core for each of the halogens; they are 0.001 61 for F, 0.050 93 for Cl, 0.104 61 for Br, and 0.3104 for I. The parameters α_i^l and r_c are fitted to optimize agreement between the calculated energy levels of H_V and the experimental levels [18–20] of the charge 6+ ion. We list our values for α_i^l and r_c in Table I. There is much less experimental data on these halogen ions to fit compared to previous studies of the alkaline earths, which may introduce larger errors into α_i^l and r_c. However, we suspect that the relatively large number of valence electrons explicitly described in the calculation will tend to diminish the effect of errors in the one-electron potential. The last term of H represents the interaction of electron i with the dipole moment of the core induced by electron j [21]. This form of the dielectronic interaction has been chosen so that this term will cancel the polarizability term in Eq. (3) when the valence electrons are configured to have zero total dipole moment. Both terms in the potential V proportional to the polarizability of the inner core are small but can have a non-negligible effect, especially in I.

C. Evaluation of multielectron matrix elements

The construction of computer code for the evaluation of multielectron matrix elements involves a nontrivial effort. To this end we have encoded an algorithm based on that described in Ref. [22(a)] with the modification that we do not try to compact the angular recoupling beyond 6-j symbols (i.e., in our program the angular parts of multielectron matrix elements are evaluated by summing products of 6-j coefficients). We feel that this level has maximum efficiency because higher-j symbols are typically calculated as sums over products of 6-j symbols anyway. As in Ref. [22(a)] we use Fano's method [22(b)]

TABLE I. Parameters for the semiempirical potential for the valence electrons.

Atom	l	α_1^l	α_2^l	α_3^l	r_c
F	0–4	8.854 87	8.755 29	17.020 01	1.0
Cl	0–4	5.212 29	16.528 51	20.157 75	0.3
Br	0	7.782 13	71.534 05	4.780 54	0.6
	1	8.177 50	71.175 49	4.674 64	0.6
	2–4	7.257 00	71.839 20	5.098 90	0.6
I	0	5.819 97	51.927 34	3.535 95	0.5
	1	6.299 98	52.149 89	3.409 34	0.5
	2–4	6.123 30	51.846 00	3.521 30	0.5

for antisymmetrizing with respect to electrons in different shells but do not use his "orbiton" for the evaluation of the angular part of the matrix element. We debugged the program for calculating the $1/r_{12}$ matrix element by comparing our output with that from a similar program [16] which was based on calculating the angular part of the matrix element by summing products of 3-j coefficients. We found the two methods to have comparable speed for configurations with less than three shells with nonzero angular momenta or spin. Our computer program can evaluate multielectron matrix elements of a symmetric two-electron operator between states having any number of electrons and shells with up to two s, six p, ten d, two f, or two g electrons in each shell. The multielectron one-particle operators (e.g., dipole operator, H_V, and Λ) are easier to evaluate.

III. APPROXIMATE IONIC WAVE FUNCTIONS

In the next subsections we describe some of the approximations which have proved to be crucial for a successful calculation of halogen spectra which have not been needed in previous eigenchannel R-matrix calculations. These approximations have been used with good effect in other types of atomic calculations and represent the drive to compactly describe multielectron and multiconfiguration dynamics.

A. Constructing target functions

A major consideration of R-matrix calculations concerns the accurate description of target-state functions. Target states are the possible wave functions of the positive ion in the energy range of interest. For the alkaline earths (Be, Mg, Ca, . . .), this aspect of the computation is trivially satisfied (when a semiempirical model potential is used) since the target function is simply an orbital of the one-electron ionic potential [14]. For the halogens at low energy, the target states in order of increasing energy are $ns^2np^4\,{}^3P_{2,1,0}$, ${}^1D_2$, and ${}^1S_0$. Of course, more effort goes into determining multielectron target functions which magnifies the amount of work needed to describe the full atomic dynamics.

The halogen ion of charge $1+$ can be very well described in a Hartree-Fock formulation [5]. This simplification is what makes the computation feasible. However, the R-matrix procedure obtains its greatest efficiency when the variational parameters are linear parameters (i.e., coefficients of basis functions). This forces us to use a three-step procedure when computing the Hartree-Fock portion of the target function.

The first step consists of solving the Hartree-Fock equations for six interacting electrons moving in the model potential (of the charge $7+$ ion), to determine the ns and np orbitals of the ns^2np^4 core wave function. We use the "average" equations obtained by summing the three different LS couplings. Next, in a second step, we construct a local s potential and a local p potential which give the Hartree-Fock ns and np orbitals as solutions. The difference between the orbitals in the fitted potentials and the Hartree-Fock orbitals is always less than a percent. This discrepancy has a negligible effect since the eigenchannel R matrix is a variational procedure, and since these fitted potentials are only used to generate a basis set. To distinguish this l-dependent potential from the one discussed in Sec. II, we will call it $\bar{V}$. Finally, in the R-matrix calculation we use the potential $\bar{V}$ to generate the single-electron orbitals. This procedure modestly complicates the single-electron portion of the Hamiltonian because we must now include the off-diagonal matrix elements of $V-\bar{V}$, but the savings in effort obtained by using physically relevant basis functions vastly outweighs this complication.

Concerning the procedure described in the preceding paragraph, it is worth noting that the first two steps of this algorithm are not very difficult; they require only a minute or two of CPU time on a small workstation. Also they are independent of the many-electron variational calculation and thus can be implemented as a separate program independent of any R-matrix program (i.e., $\bar{V}$ does not depend on the total initial- nor final-state wave function). A second point is that the d and f contribution to $\bar{V}$ are dictated by very different physical considerations discussed next.

B. $n\bar{d}$, $4\bar{f}$ natural orbitals

The dominant core configurations $ns^2np^4(L_cS_c)$ of the halogen ion contribute $\sim 95\%$ of the configuration-interaction (CI) target state. The rest of the wave function contains contributions from terms such as $nsmsnp^4$, ns^2np^3mp, $nsnp^4md$, $ns^2np^2md^2$, ns^2np^3mf, ... We cannot use a brute force approach including, for example, all of the different m's implied by $nsnp^4md$ in the full atomic basis function because of the huge number of one- and two-electron excitations of the core. The full atomic wave function is much more complicated because each of the terms of the target is coupled to a superposition of orbitals representing the wave function of a highly excited electron near the core. A small reduction in the number of core configurations needed to describe the target state will result in a large reduction in the number of basis functions needed to describe the atomic state.

However, it is possible to first sum all of the md orbitals to make an $n\bar{d}$ orbital [5,23] which will contain the major contribution of $nsnp^4md$ and $ns^2np^2md^2$ to the target function. This idea was introduced by Löwdin and has been implemented by Froese-Fischer. A similar procedure can be followed to obtain a $4\bar{f}$ orbital, as well as an $(n+1)\bar{s}$ and $\bar{p}$. These "natural" orbitals are absolutely crucial to the success of the calculations; the summation which constructs the natural orbitals occurs at an initial step of the calculation and thus we greatly reduce the number of multielectron basis function (as well as matrix elements) needed for convergence. By creating natural orbitals we include the most important corrections to the Hartree-Fock target states in the most compact, physical way possible. We describe below the algorithm which we used to incorporate the natural orbitals into our R-matrix program.

The major difference between the barred and unbarred d and f orbitals consists of the barred orbitals being drawn to much smaller radii. At first sight this may seem

paradoxical because the added localization increases the kinetic energy of the $\bar{d},\bar{f}$ electron. However, the increase in energy due to localization is small compared to the lowering of the ground-state energy by maximizing the off-diagonal $1/r_{ij}$ interaction. To see how this occurs, note that the contribution to the total energy from the kinetic energy of the natural orbitals is proportional to ε^2 (where ε is the amplitude for mixing the terms containing natural orbitals into the wave function) while the contribution to the total energy from the off-diagonal $1/r_{ij}$ interaction is proportional to ε. (The splitting between two levels increases when their off-diagonal matrix element increases in magnitude; therefore the lower level decreases in energy when the off-diagonal matrix element increases in magnitude.) For the halogen atoms, ε is a small number due to the Hartree-Fock character of the target states. The off-diagonal interaction can be increased by pulling the $n\bar{d}$ and $4\bar{f}$ orbitals to smaller radii where they will have a larger overlap with the ns,np orbitals. The characteristics of the $n\bar{d}$ and $4\bar{f}$ orbitals can also be rationalized from a coupled channel picture; the wave function only mixes in higher l components at radii where there is already substantial amplitude for finding an electron.

In practice, we obtain the $n\bar{d}$ and $4\bar{f}$ orbitals recursively. We begin by constructing a large configuration-interaction matrix which has the target basis functions ns^2np^4, $nsmsnp^4$,. ns^2np^3mp, $nsnp^4md$, $ns^2np^2md^2$, ns^2np^3mf,. . . . We obtain the coefficients of each basis function by diagonalizing this configuration-interaction matrix for the target state. Finally, we superpose the md and mf orbitals using these coefficients to obtain orbitals proportional to the natural $n\bar{d}$ and $4\bar{f}$ orbitals. We then *construct* a d potential and an f potential which very nearly give the natural orbitals as eigenstates, thus completing the determination of $\bar{V}$. This potential has the same form as V in Eq. (3) with 7 replaced by 2 and α_i^l replaced by $\bar{\alpha}_i^l$. The $\bar{\alpha}_i^l$ which we obtained are listed in Table II. The advantage of this recursive method is the consequential rapid decrease of the natural orbitals' coefficients. For example, the coefficients of the $4s4p^4(^1D)md\ ^3P$ basis functions of the ^3P CI target state of Br are 0.071, −0.061, 0.047, −0.030, 0.017 for $m=4,5,6,7,8$; when we use basis functions constructed from the natural orbitals [i.e., $4s4p^4(^1D)m\bar{d}\ ^3P$], the coefficients are 0.106, 0.004, −0.002, 0.001, 0.000 for $m=4,5,6,7,8$. Figure 1 shows the f and $4\bar{f}$ orbitals for the Cl calculation. Also graphed in this figure is the $3p$ orbital, which gives an indication of its large radial overlap with the natural orbital.

TABLE II. Parameters for the semiempirical potential for the natural orbitals.

Atom	l	$\bar{\alpha}_1^l$	$\bar{\alpha}_2^l$	$\bar{\alpha}_3^l$	r_c
F	0,1	2.034 42	−5.365 89	3.762 26	1.0
	2	6.853 21	23.299 75	1.510 06	1.0
	3,4	7.161 05	25.040 65	1.018 00	1.0
Cl	0	1.539 23	−26.612 80	2.956 85	0.3
	1	1.724 25	−28.505 27	3.575 66	0.3
	2	0.740 85	−34.693 71	2.198 70	0.3
	3,4	0.579 00	−44.035 09	2.553 09	0.3
Br	0	4.944 51	27.887 10	2.429 00	0.6
	1	5.116 79	27.771 50	2.338 48	0.6
	2	4.325 36	12.762 76	1.061 01	0.6
	3,4	3.640 40	8.037 92	0.657 67	0.6
I	0	4.759 81	33.419 64	2.221 07	0.5
	1	5.144 17	35.332 26	2.158 23	0.5
	2	4.502 57	16.902 31	1.180 06	0.5
	3,4	3.867 99	5.931 59	0.551 83	0.5

The coefficients of our configuration-interaction wave functions for Cl^+ are similar to those in Ref. [5]. For example, the coefficients of the most important ^1S configurations which we (they) obtain are 0.183 $(0.181)3p^6$, 0.144 $(0.150)3s^23p^2\ ^1S, 3\bar{d}^2\ ^1S$, and −0.095 $(-0.101)3s^23p^2\ ^1D, 3\bar{d}^2\ ^1D;\ ^1S$. Reference [5] does not use configurations which contain $4\bar{f}$ orbitals; we found the coefficient of these configurations to be ~0.05. In Table III we give our calculated target-state energies as well as LS-averaged experimental threshold energies [24]. The relative error in our calculation is always less than 10%. Our calculated ionization thresholds are too small by 5–10%, indicating that the ground state is not converged as well as the target states which is not surprising since our one-electron orbitals were developed for the target states.

IV. SPIN-ORBIT INTERACTIONS

The eigenchannel R-matrix approach provides the logarithmic derivative of the wave function at a given energy at the surface of the R-matrix volume. This information together with the value of the wave function at the surface completely determines the wave function everywhere outside of the R-matrix volume. The wave function outside can be written in the form

$$\psi_i=\mathcal{A}\sum_j \Phi_j(\Omega)[f_j(r)\delta_{ji}-g_j(r)K_{ji}^{(LS)}]\ , \tag{4}$$

where $\mathcal{A}$ is the antisymmetrization operator (which has no practical effect at $r>r_0$ since the outer electron does not occupy the same region of space as the core electrons), $\Phi_j(\Omega)$ represents the target function and the LS coupling of the target's angular momenta with that of the outer electron to give L and S, and $\underline{K}^{(LS)}$ is the short-

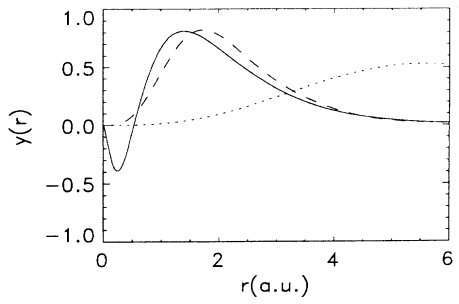

FIG. 1. $4\bar{f}$ (dashed line) and $4f$ (dotted line) orbitals of Cl^+. The $3p$ orbital (solid line) is shown for comparison.

TABLE III. Theoretical and experimental J-averaged target-state energies in atomic units.

Atom	Theor. ^3P	Theor. ^1D	Theor. ^1S	Expt. ^3P	Expt. ^1D	Expt. ^1S
F	0.0000	0.0985	0.2138	0.0000	0.0943	0.2038
Cl	0.0000	0.0563	0.1353	0.0000	0.0513	0.1252
Br	0.0000	0.0494	0.1238	0.0000	0.0457	0.1161
I	0.0000	0.0408	0.1031	0.0000	0.0374	0.0998

range reaction matrix [14]. Open and closed channels are included in Eq. (4); thus the ψ_i contain terms which are exponentially diverging at $r \to \infty$. This startling property ensures the slow energy dependence of $\underline{K}^{(LS)}$, because $\underline{K}^{(LS)}$ only depends on the dynamics inside of the R-matrix volume where interaction energies are large. The physical reaction matrix which results from superposing ψ_i to eliminate the exponentially diverging terms has a much more rapid energy dependence, as is familiar from other MQDT studies.

The reaction matrix in Eq. (4) has the superscript LS to denote that it depends on the total spin and orbital angular momenta. $\underline{K}^{(LS)}$ is a completely nonrelativistic quantity. Each of the reaction matrices constitutes one block of a larger block-diagonal total reaction matrix

$$\underline{K} = \begin{bmatrix} \underline{K}^{(LS)} & 0 & \cdot \\ 0 & \underline{K}^{(\bar{L}\,\bar{S})} & \cdots \\ \vdots & \vdots & \ddots \end{bmatrix} . \tag{5}$$

The block-diagonal nature of $\underline{K}$ is strictly an approximation, the error (which should be small) being due to our neglect of relativistic effects within the R-matrix volume. The reaction matrix of Eq. (5) and the dipole transition matrix represent all of the dynamical information needed to describe the atomic system. These parameters quantify the degree of similarity between different atomic systems better than the photoabsorption spectra themselves.

$\underline{K}$ contains the dynamical information appropriate when the atomic system is best described by an LS angular-momentum coupling. This coupling can be represented by the ket $|[(L_c l_o)L(S_c s_o)S]J\rangle$, in which (a) the total orbital angular momentum of the core, L_c, is coupled to the orbital angular momentum of the outer electron, l_o, to give the total orbital angular momentum L; (b) the total spin of the core, S_c, is coupled to the spin of the outer electron, $s_o = \frac{1}{2}$, to give the total spin S; and (c) L and S are coupled to give the total angular momentum J. This coupling scheme is appropriate when the electron is near the core, since the dominant electrostatic and exchange interactions are diagonal in this representation. However, when the electron leaves the core the LS dependence of these forces quickly becomes negligible [14].

Once the electron leaves the core region, it is only affected by a long-range Coulomb interaction which is the same for all target states. The electron's rate of phase accumulation depends on the target state only through the energy difference of these states; the energy available to the outer electron equals the total energy minus the energy of the core. The energy of the target state does not depend on L_c and S_c alone but on the total angular momentum of the core, J_c. This implies that the jj angular coupling scheme is more appropriate when the electron is outside of the core region, and should be represented by the ket $|[(L_c S_c)J_c(l_o s_o)j_o]J\rangle$. Actually, any angular-momentum coupling in which $L_c S_c$ is coupled to J_c would be equally appropriate (i.e., jK or $J_c J_{cs}$ coupling). The reaction matrix in this jj-coupled representation can be obtained from the LS-coupled $\underline{K}$ matrix by a simple orthogonal transformation. The transformation matrix

$$U_{jj,LS} = \langle [(L_c S_c)J_c(l_o s_o)j_o]J | [(L_c l_o)L(S_c s_o)S]J \rangle \tag{6}$$

is simply the projection of one type of coupling onto the other which involves a Racah 9-j coefficient. Explicitly,

$$\underline{K}_{jj} = \underline{U}\,\underline{K}\,\underline{U}^{\dagger} , \tag{7}$$

$$\underline{d}_{jj} = \underline{d}_{LS}\underline{U}^{\dagger} . \tag{8}$$

This is of course an approximation which is accurate as long as $\underline{K}$ does not appreciably vary over an energy range comparable to the fine-structure splittings of the core. The rotation matrix $\underline{U}$ does not depend on the strength of relativistic effects and thus the transformations (7) and (8) represent couplings in the K matrix of zeroth order in the relativistic interactions. The terms omitted in Eq. (5) are of first order. These couplings only have a strong effect on the Rydberg levels which have an orbital frequency comparable to or larger than the fine-structure splitting. When the approximations embodied by Eqs. (5)–(8) hold, the simpler LS coupling calculation which totally ignores spin-orbit effects will reproduce the experiment if the fine-structure splitting of the thresholds is smaller than the experimental resolution. We use the *experimentally* determined ionization threshold energies [24] when we apply the MQDT boundary conditions with the relativistic $\underline{K}$ matrix and dipole transition operator, Eqs. (7) and (8). These threshold energies are the only experimentally determined parameters of the neutral atom which we use in our calculation; of course, we use the experimental energy levels of the charge 6+ ion in the determination of the valence Hamiltonian, Eq. (3).

The transformation Eqs. (6)–(8) can be thought of as a geometric rotation because $\underline{U}$ is the same for all of the halogens. This type of frame transformation has been successfully applied to the spectra of the alkaline earths [14] and to the rare-gas atoms [9,10(a)]. For the halogens, as well as for atoms in all other columns of the periodic table, there is an additional coupling whose effect has not been previously studied. In particular, for all atoms except those with only a single electron or hole in the target valence shell, the $\mathbf{l}_i \cdot \mathbf{s}_i$ interaction not only splits the states having the same $L_c S_c$ but different J_c but also *couples* the states with different $L_c S_c$ but the same J_c. In the halogens this coupling mixes the $ns^2np^4(^3P_0)$ with $(^1S_0)$, and $(^3P_2)$ with $(^1D_2)$. The coupling varies from atom to atom because it depends on the strength of the $\mathbf{l}_i \cdot \mathbf{s}_i$ interaction as well as the energy differences between the different $L_c S_c$ states. The nonadiabatic coupling represented by this dynamical frame transformation allows the $^1Dmd\,^2S^e_{1/2}$ states above the $^3P_0$ threshold to

TABLE IV. Rotation angles (in rad) for the dynamical frame transformation.

Atom	θ_2	θ_0
F	0.011	−0.011
Cl	0.041	−0.036
Br	0.166	−0.167
I	0.317	−0.396

autoionize to the $^3P_2\epsilon d\ ^2P_{1/2}$ continuum (i.e., the decay occurs through the fine-structure interaction of the $^3P_2$ *target* state with the $^1D_2$ target state). The $^1Dmd\ ^2S^e$ states would *not* autoionize if we only applied the usual *LS*-to-*jj* frame transformation because the singlet thresholds do not have a fine-structure splitting, at least in the energy range above the $^3P_0$ threshold. The geometric frame transformation has no effect on the total cross section when none of the thresholds of the closed channels have a fine-structure splitting. These resonances are absent from previous *LS*-coupled photoionization calculations, such as that of Ref. [6].

An *ab initio* determination of the mixing angles in the dynamical frame transformation is very difficult due to the contribution from the other valence electrons to the spin-orbit coupling. To obtain the mixing angles we take advantage of the fact that the target states are ~95% ns^2np^4 which implies that the radial matrix element in the fine-structure interaction will be the same for all of the different states. Therefore

$$\langle ns^2np^4\,{}^SL_J|V_{\rm SO}|ns^2np^4\,{}^{\bar S}\bar L_{\bar J}\rangle = y_n\langle p^4\,{}^SL_J|\mathbf{l}\cdot\mathbf{s}|p^4\,{}^{\bar S}\bar L_{\bar J}\rangle$$

should be a good approximation. We now fit y_n and three *LS* energies to the experimental ionization energies to obtain the two mixing angles θ_0 and θ_2. The lower-energy state of total angular momentum J is $|ns^2np^4\,{}^3P_J\rangle\cos\theta_J+|ns^2np^4\,{}^1J_J\rangle\sin\theta_J$ and the higher-energy state is $-|ns^2np^4\,{}^3P_J\rangle\sin\theta_J+|ns^2np^4\,{}^1J_J\rangle\cos\theta_J$. Table IV gives the values of θ_J which we have obtained by this method. This procedure is analogous to the "intermediate-coupling" method of Berkowitz and Goodman [25]. The angles they obtain are within 10% of our values except those for Cl, which are 0.01 rad smaller in magnitude than our values [25(a)].

The dynamical frame transformation provides a good approximation to the dynamics as long as the K matrix does not appreciably vary over an energy range comparable to the energy splittings of the core, i.e., the $^3P_2$-$^1D_2$ splitting and $^3P_0$-$^1S_0$ splitting. Unfortunately, near the ^3P_J thresholds the ^1Smd and ^1Sms channels are strongly, rather than weakly, closed which causes the dynamics in the $^2D^e$ and $^2S^e$ final-state symmetries to vary more quickly than at higher energies. This circumstance may account for the unexceptional agreement between our calculated and the experimental cross sections between the $^3P_2$ and $^3P_0$ thresholds in Br and I.

V. COMPUTATIONAL DETAILS

The halogen-atom ground state can be represented well by a Hartree-Fock wave function of the type $ns^2np^5\,{}^2P^o$. However, we have used the *ns* and *np* orbitals to describe the Hartree-Fock orbitals of the ionic state which are slightly compressed compared to the orbitals for the neutral atom. This circumstance forces us to include many basis functions which primarily represent this simple relaxation (i.e., functions like $[nsms\ {}^1S]np^5$, ns^2np^4mp, etc.). We also include correlation effects in the ground-state basis function, which necessitates many more basis functions than for rare-gas atoms because the halogen ground state has nonzero spin and angular momentum. The main effects emerge from calculations with less than 50 basis functions for the ground state, but we include many more basis functions than this in order to achieve the maximum possible agreement between the cross sections calculated in the length and velocity gauges for I. We did not modify our choice of basis functions for the different atoms, although the radial orbitals differed of course from one halogen to another. The ground state was composed of ~300 basis functions with ~90 different angular configurations. The most important angular configurations were ns^2np^5, ns^2np^4mp, $nsmsnp^5$, $nsnp^5md$, ns^2np^4mf, np^5md^2, $ns^2np^3md^2$, and np^6mp. All possible intermediate angular couplings are used for each shell configuration. For example, ns^2np^4mp means each of the three possible couplings: $[(ns^2\,{}^1S)(np^4\,{}^1S)^1S]mp$, $[(ns^2\,{}^1S)(np^4\,{}^3P)^3P]mp$, and $[(ns^2\,{}^1S)(np^4\,{}^1D)^1D]mp$. The disagreement between the cross sections calculated in the length and velocity gauges is typically less than 10% for all of the halogen atoms which gives an indication of the convergence of both the ground-state and final-state wave functions.

There are seven different final-state *LS* symmetries and 15 total final-state channels which enter our calculation (in what follows the three *LS*-coupled core states $ns^2np^4\,{}^3P$, $ns^2np^4\,{}^1D$, and $ns^2np^4\,{}^1S$ will be shortened to ^3P, ^1D, and ^1S, respectively): $^1Dmd\ ^2S$, $^1Sms\ ^2S$, $^3Pms\ ^2P$, $^3Pmd\ ^2P$, $^1Dmd\ ^2P$, $^1Dms\ ^2D$, $^3Pmd\ ^2D$, $^1Dmd\ ^2D$, $^1Smd\ ^2D$, $^3Pmd\ ^2F$, $^1Dmd\ ^2F$, $^3Pms\ ^4P$, $^3Pmd\ ^4P$, $^3Pmd\ ^4D$, and $^3Pmd\ ^4F$. The largest basis-set sizes were ~700 for the ^2D final-state symmetry and ~450 for the ^2P final-state symmetry. For the final-state symmetries we could decrease the basis-set size by a factor of 2–3 and still obtain reasonable results, whereas for the ground-state symmetry a decrease by a factor of 8 in the basis-set size still gave adequate results. Part of the reason for the large basis-set size was that the basis was chosen to give converged results for I which made necessary the inclusion of basis functions unnecessary for the lighter halogens. Our results for the $^2D^e$ final-state symmetry of Cl using ~450 basis functions were completely indistinguishable from the larger calculation.

The complete calculation of the photoionization cross section for one atom including the computation of the ground-state wave function and *LS*-to-*jj* frame transformation required ~2.5 h of CPU time on a DEC station 5000/200 computer.

VI. RESULTS

A. Cross sections

Figures 2–10 present the current theoretical calculations and the experimental results where available. In

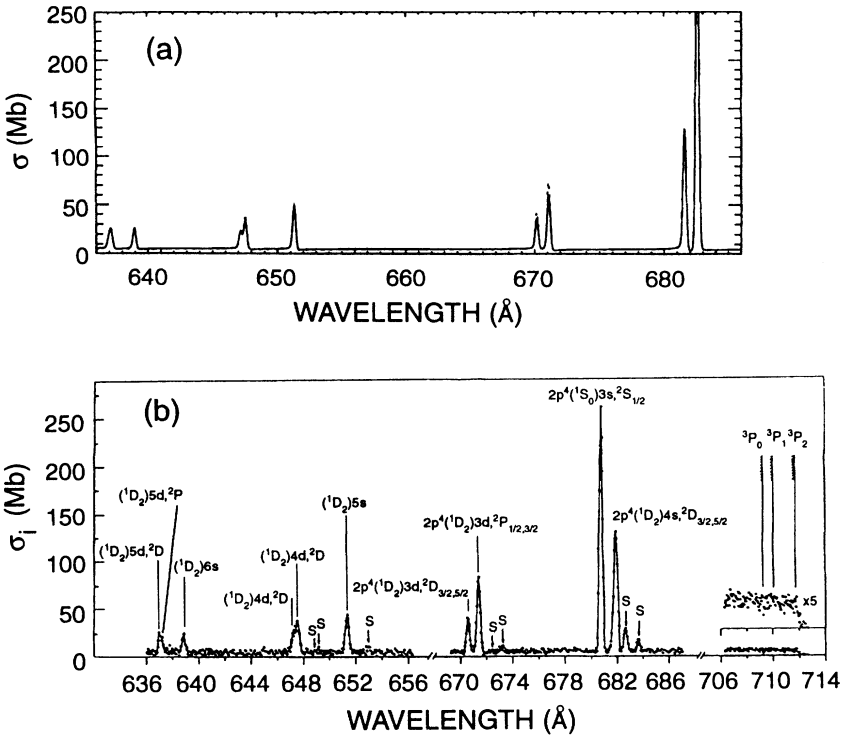

FIG. 2. Photoionization cross section of the $^2P_{3/2}$ ground state of F between the ^3P and ^1D thresholds. (a) Calculated length (solid line) and velocity (dashed line) gauge cross sections have been convolved with the quoted experimental resolution of 0.28 Å. (b) Experimental cross section [1]. (The peaks marked with an S are from the photoionization of the $2s^22p^5\,^2P_{1/2}$ excited state.) The two calculated peaks at ~682 Å are in the opposite order compared to experiment.

general there is good agreement between the two. Possibly the most striking feature of these figures is the huge difference between F (Figs. 2 and 3) and the other halogens, as well as the remarkable similarity between Cl (Figs. 4 and 5), Br (Figs. 6–8) and I (Figs. 9 and 10). The reason for the absence of broad features in F can be traced to the lack of overlap between a d electron and the inner p core. These broad features in the heavier halogens are ^1Dmd autoionizing resonances which decay primarily into the $^3P\varepsilon d$ continuum channels. Figure 11 shows the $2p$ and $3d$ orbitals for F and the $3p$ and $3d$ orbitals for Cl. Notice the much larger overlap in Cl. The md states of F are sharper (i.e., longer lived) because there is only a small amplitude for this d electron to get near enough to the core to inelastically scatter. This argument explains why all of the nd autoionizing levels in the first-row atoms are sharp. Similar reasoning shows why the dipole transition strengths $np \rightarrow md$ and $np \rightarrow ms$ are comparable in F, but in the heavier halogens $np \rightarrow md$ dominates according to the expected propensity rule for photoabsorption [26].

Figures 2, 4, 7, and 9 show the photoioinization cross section for all of the halogen atoms between the ^3P and ^1D thresholds. The broad resonances are a superposition of two broad autoionizing series, $^1Dmd\,^2P^e$ and $^1Dmd\,^2D^e$. These resonances were misclassified in some early studies [2] of Cl but have since been correctly reclassified [3,27]. The sharp resonance peak at longer wavelengths is always $^1Dms\,^2D^e$ which decays through its coupling to the $^3P\varepsilon d\,^2D^e$ continuum and the one at shorter wavelengths is $^1Dmd\,^2S^e$ which decays due to the

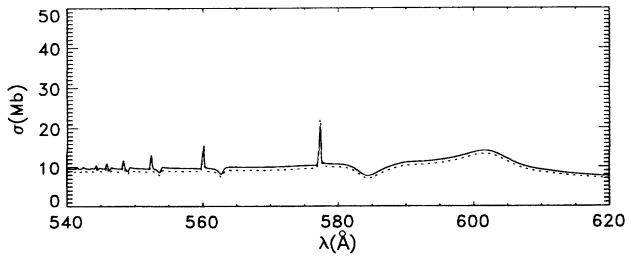

FIG. 3. Calculated length (solid line) and velocity (dashed line) gauge photoionization cross section of the $^2P_{3/2}$ ground state of F between the ^1D and ^1S thresholds.

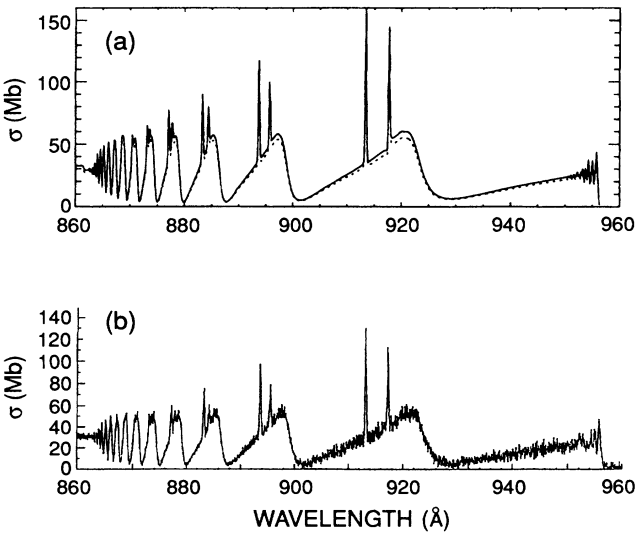

FIG. 4. Same as Fig. 2 but for Cl (Ref. [2]) between the ^3P and ^1S thresholds.

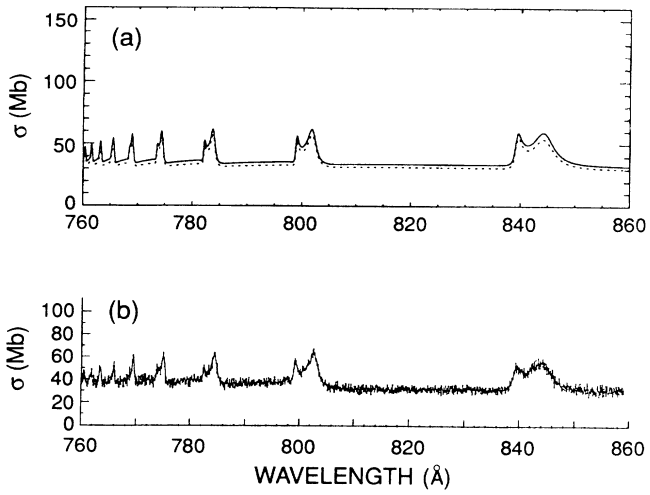

FIG. 5. Same as Fig. 3 but for Cl (Ref. [2]) between the ^1D and ^1S thresholds.

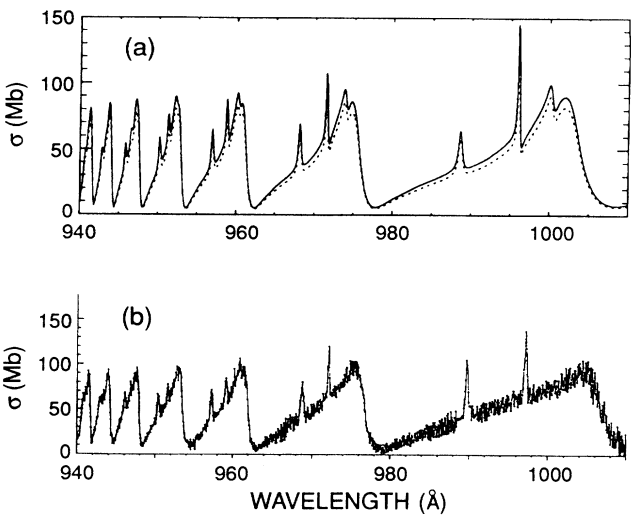

FIG. 7. Same as Fig. 2 but for Br (Ref. [3]) between the $^3P_0$ and ^1D thresholds.

spin-orbit coupling of the $^3P_2$ target state to the $^1D_2$ target state. The window resonance at the peak of the sawtooth is $^1Dmd\ ^2F^e$. These classifications hold for all of the heavier halogen atoms. All of these resonances are present in the same relative order and with the same shape in Cl, Br, and I. The depths of the $^1Dmd\ ^2F^e$ resonances depend upon the strength of the relativistic spin-orbit coupling which is weakest for Cl and strongest for I, but its width derives from its coupling to the $^3P\varepsilon d\ ^2F^e$ continuum which is nearly the same in the three different atoms. The $^2F^e$ window resonance is not apparent in the experimental Br spectrum but quite visible in the calculated spectrum. It is possible that this structure is hidden in the noise. Above the ^1D threshold there are two series

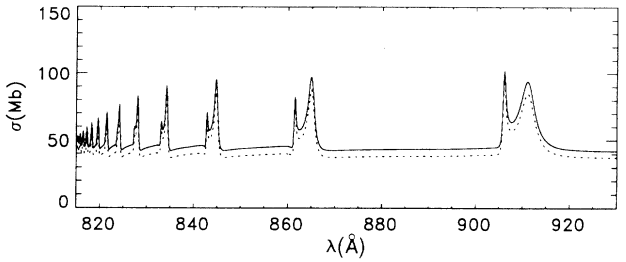

FIG. 8. Same as Fig. 3 but for Br between the ^1D and ^1S thresholds.

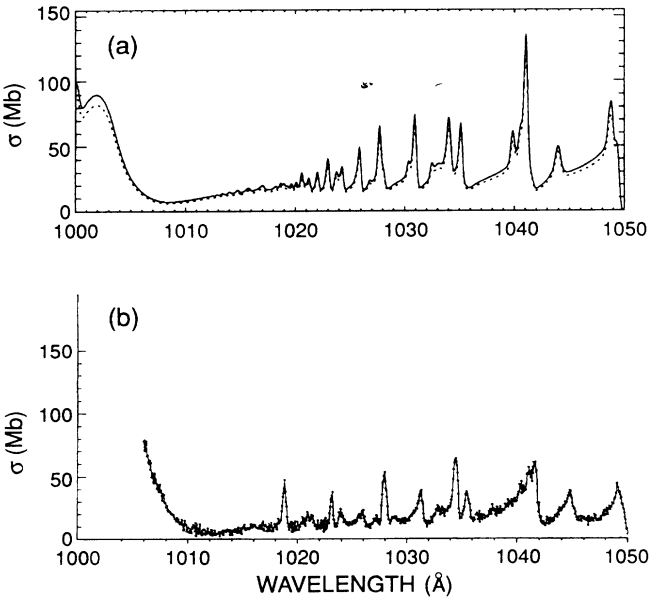

FIG. 6. Same as Fig. 2 but for Br (Ref. [3]) between the $^3P_2$ and $^3P_0$ thresholds.

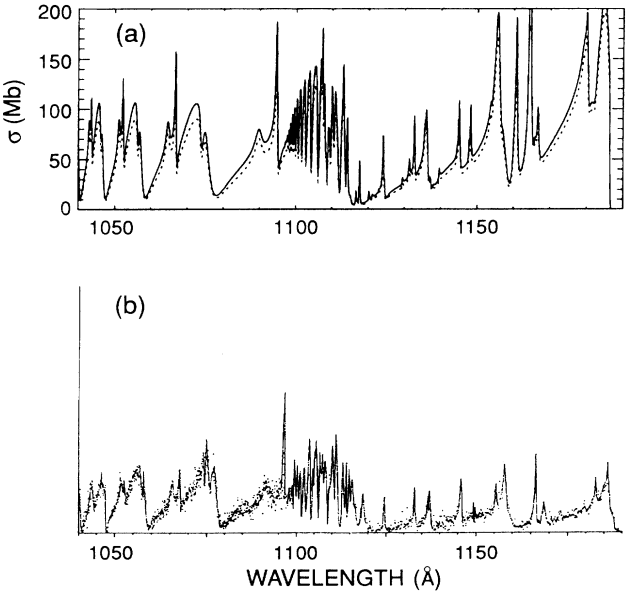

FIG. 9. Same as Fig. 2 but for I (Ref. [4]) between the $^3P_2$ and ^1D thresholds.

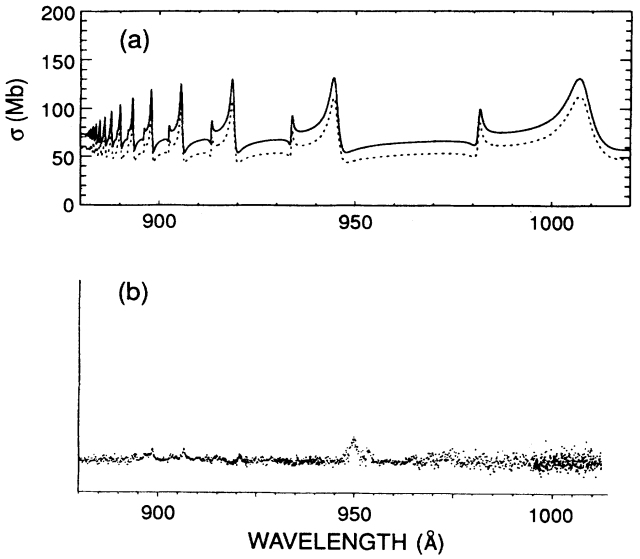

FIG. 10. Same as Fig. 3 but for I (Ref. [4]) between the ^1D and ^1S thresholds.

approaching the ^1S threshold (Figs. 3, 5, 8, and 10). The $^1Sms\ ^2S^e$ series is the sharper one at shorter wavelengths and the $^1Smd\ ^2D^e$ series is the broader except in F.

In F (Fig. 3) there is an extra peak at $\sim$600 Å which we identify as the $2s2p^6\,^2S^e$ level, that has apparently not been observed or calculated. Reference [3] estimated this level to lie near 580–590 Å. The corresponding $nsnp^6$ level in the heavier atoms lies in the discrete part of the spectrum and is heavily mixed with the $ns^2np^4(^1D)nd\ ^2S$ level. Our lowest ^2S bound level in Cl is $\sim$50% $3s3p^6$ and 50% $3s^23p^43d$. Another striking difference between the halogens is the fact that the $^1Sms\ ^2S^e$ resonant peaks in the heavier halogens become *window* resonances in F due to their interaction with the broad $2s2p^6$ autoionizing level. This interaction facilitates their decay into the open $^1D\varepsilon d\ ^2S^e$ channel which is why they are anomalously broad (especially the window resonance at 585 Å). In Fig. 12, the effect of this resonance is apparent.

There is a discrepancy in the widths of the two sharp resonance $\sim$915 Å in Cl between previous calculations and experiment. Experiment [27] has determined the width of these resonances to be ≤ 0.04 Å while the previous calculations [28] give widths ≥ 0.1 Å and in one case

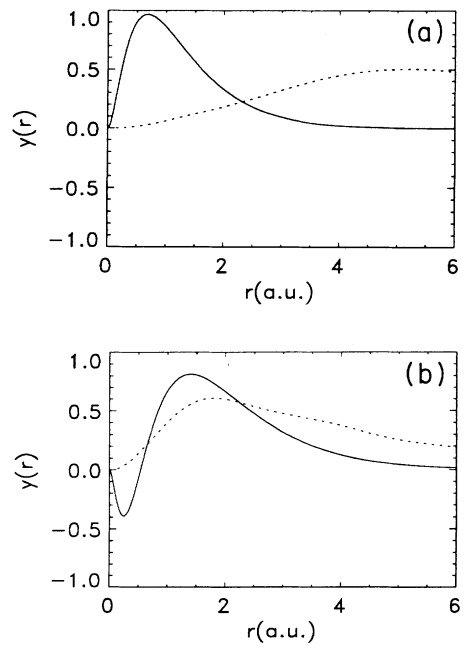

FIG. 11. Comparison of the lowest p (solid line) and d (dashed line) Hartree-Fock orbitals in F and Cl illustrating the much larger overlap between these orbitals for the heavier halogen atoms. (a) F and (b) Cl.

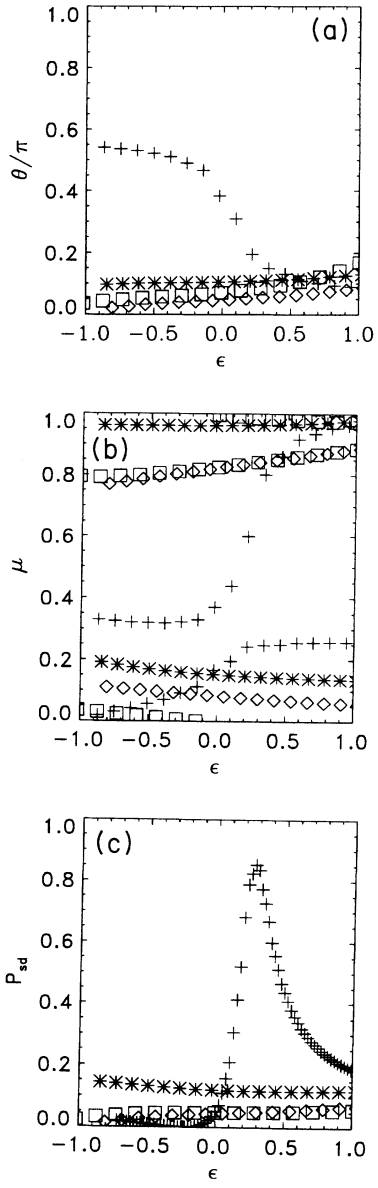

FIG. 12. MQDT parameters of the $^2S^e$ final-state symmetry for the different halogen atoms as a function of the scaled energy ϵ which is zero at the ^1D threshold and one at the ^1S threshold. (a) Mixing angle θ, (b) quantum-defect eigenvalues, and (c) probability of inelastic scattering, Eq. (10). F (+), Cl (*), Br (diamond), and I (box).

~ 0.2 Å (the experimental positions are ~ 913.17 Å for the $^1D4d\ ^2S^e$ resonance and ~ 917.25 Å for the $^1D6s\ ^2D^e$ resonance). Our calculations agree with the experimental results, giving positions (widths) of 913.43 (0.02 Å) and 917.68 Å (0.007 Å).

The calculated ionization spectra agree well with the experimental results for all of the halogens. For Cl we obtain the best agreement with experiment, with our results being nearly identical to the experiment. Since the normalization of the experimental spectrum of Ref. [2] below the ^1S threshold was obtained by equating the experimental cross section at the ^1S threshold to an average of several theoretical results, we have an indirect comparison with previous calculations. Our value for the cross section at the ^1S threshold agrees well with the three highest calculations and is slightly smaller than the experimental value of 43.6 Mb obtained in Ref. [29].

Our results agree with those of Brown, Carter, and Kelly [6] for Cl except in those instances mentioned above where our results are closer to experiment. However, the difference between the two calculations is slight. The only other calculations in this energy range are those of Lamoureux and Combet Farnoux [7] for Cl which do not include all of the important channels necessary for a complete description of the spectra in this energy range. For the channels they do include, their results are in moderate agreement with ours. The other important point of comparison is the total cross section at the ^1S threshold in Cl. Our value of the cross section is 38.5 ± 2.0 Mb where we have used the discrepancy between our length and velocity results to estimate our error. This should be compared to the theoretical values of 25 Mb of Ref. [8], 30 Mb of Ref. [5], 35 Mb of Ref. [7], 37 Mb of Ref. [6], and 39 Mb of Ref. [30] and the experimental results of 43.6 ± 3.5 Mb of Ref. [29] which was normalized to $\frac{1}{2}$ of the molecular cross section between 300 and 450 Å. Our results are smaller than those of Ref. [8(b)] at the ^1S threshold except for F where we are in agreement. Our values are ~ 40 Mb for Cl, ~ 50 Mb for Br, and ~ 70 Mb for I, compared to the Ref. [8(b)] values of ~ 60 Mb for Cl, ~ 70 Mb for Br, and ~ 90 Mb for I. Combet Farnoux and Ben Amar [31] have calculated the values of 43 Mb (31 Mb) for I at the ^1S threshold in the length (velocity) gauge. We do not know of calculations or experiments for any of the other halogen atoms in the energy range which we covered. Recent experimental work [32,33] covering the energy range below the $nsnp^5$ thresholds also shows interesting structures in the total cross sections as well as in the photoelectron asymmetry parameter β.

We now turn to the discrepancies between the experiments and our calculations. The biggest visual error in F is the $2s^2 2p^4\ ^1S\ 3s$ resonance at ~ 682.5 Å in the calculation compared to ~ 680.7 Å in the experiment which causes a reversal in the calculated order of the two autoionizing resonances near 680 Å. This discrepancy corresponds to an error of ~ 0.01 in the calculated quantum defect and an error of ~ -0.05 eV in the position of the resonance relative to the ground state. Based on several previous calculations for the alkaline-earth atoms [14], we do not expect accuracy better than this, particularly in view of the approximations made and in view of the errors in the calculated ionic levels in Table III. The error in the energy level is magnified by the small value of the effective quantum number for this resonance, $\nu\sim 1.67$. The experimental height of this level is about $\frac{5}{8}$ the calculated height after convolution with the experimental resolution. From the dynamical frame transformation we estimate that the width of this level should be ~ 0.002 Å which would correspond to a resolved peak height of $\sim 30\,000$ Mb. This width implies an autoionization lifetime of order 10^{-11} sec. Berry *et al.* [34] measured a mean lifetime of $(3\pm 1)\times 10^{-10}$ sec for this state which is a factor of 30 larger than what we estimated, indicating a breakdown of the dynamical frame transformation. By a comparison with two calculated decay rates by radiation, they estimate that this state autoionizes approximately three times faster than it radiates. If we use this branching ratio to correct our peak height we obtain good agreement with the value of Ref. [1]. The discrepancies in Br (Figs. 6 and 7) result from the broad $^1Dmd\ ^2P^e$, $^2D^e$, and $^1Smd\ ^2D^e$ resonances being shifted too high in energy by a quantum defect error of ~ 0.05. This error is perhaps slightly larger than expected. The agreement of our I calculations with experiment is good but not great. Certainly, a large part of the error can be traced to our inadequate treatment of the dynamical frame transformation. Br and, especially, I are conspicuous by the inadequate experimental spectra of the charge 6+ ion needed to determine the one-electron valence potential needed for our calculations. We are uncertain about how large an effect the errors in the valence potential can have on the theoretical spectrum.

B. MQDT parameters

Another measure of similarity and contrast between the different halogens can be obtained by an examination of the reaction (reactance) matrix, especially quantum defects μ_α and mixing angles θ. Due to the large number of final-state symmetries we will focus on these properties for only two of the LS symmetries, $^2S^e$ and $^2P^e$. To facilitate comparison between the different atoms we will plot the μ_α and θ versus a scaled energy ϵ which will be zero at the $ns^2np^4\ ^1D$ threshold and one at the $ns^2np^4\ ^1S$ threshold.

The first symmetry we consider is the $^2S^e$ symmetry which has two channels, $ns^2np^4\ ^1S\varepsilon s$ and $ns^2np^4\ ^1D\varepsilon d$, which will be denoted the s and d channels. The important parameters which describe the interaction between these channels are the mixing angle θ and the quantum-defect eigenvalues μ_1 and μ_2, [13], given by

$$\begin{bmatrix} K_{ss} & K_{sd} \\ K_{ds} & K_{dd} \end{bmatrix} \begin{bmatrix} \cos\theta & -\sin\theta \\ \sin\theta & \cos\theta \end{bmatrix} = \begin{bmatrix} \cos\theta & -\sin\theta \\ \sin\theta & \cos\theta \end{bmatrix} \begin{bmatrix} \tan\pi\mu_1 & 0 \\ 0 & \tan\pi\mu_2 \end{bmatrix} . \quad (9)$$

In Fig. 12(a) we plot the mixing angle and in 12(b) the quantum defects for the different atoms. The probability that an electron in the s channel will scatter into the d

channel (or vice versa) in one collision with the core is

$$P_{sd} = \sin^2 2\theta \sin^2 \pi(\mu_1 - \mu_2) \ . \tag{10}$$

This quantity is plotted in Fig. 12(c). It is easy to see from Eq. (10) that the maximum probability for scattering from one channel to the other obtains when $\Delta\mu$ is half integer and θ is an odd multiple of $\pi/4$.

Figure 12 shows another striking difference between F and the heavier halogens. Namely, there is a resonance in F (Fig. 3) at $\epsilon \sim 0.2$ ($\lambda \sim 603$ Å) associated with the $2s2p^6\,{}^2S$ configuration. The corresponding resonances, $nsnp^6\,{}^2S$, in all of the other halogens are at energies below the $ns^2np^4\,{}^3P$ threshold. The large *s-d* mixing in F near the resonance indicates that it decays with nearly the same rate into the *s* or *d* channels. The small $2p$-ϵd overlap inhibits decay to the *d* channel which would normally be expected to serve as the dominant escape channel. The large *s-d* mixing in the $^2S^e$ channel in F induced by the $2s2p^6$ resonance explains the anomalous width of the window resonances in Fig. 3. The mixing angles for the heavier halogens cluster near 0.55π indicating very little *s-d* mixing; complete mixing obtains at the angles $\pi/4$ and $3\pi/4$ while zero mixing obtains at the angles 0 and $\pi/2$. There is very little *s-d* mixing in any of the *LS* symmetries, which accounts for the narrow widths of all of the *ms* autoionizing resonances.

The quantum-defect eigenvalues in Fig. 12(b) again show the $2s2p^6$ resonance in F. Away from this resonance we can discern a trend in the quantum defects which reflects the changing dynamics with increased Z. Examine the μ_α near $\epsilon = -0.5$. There is one quantum defect, which we can associate with the *s* channel due to the small mixing, which decreases by ~ 0.1 going from atom to atom: F$\sim$0.3, Cl$\sim$0.17, Br$\sim$0.07, I$\sim$0.0. The other quantum defect, associated with the *d* channel, behaves slightly more erratically: F$\sim$1.05, Cl$\sim$0.95, Br$\sim$0.8, I$\sim$0.8. The difference between the quantum defects is roughly 0.75 for all of the atoms giving an *s-d* mixing probability [Fig. 12(c)] of ~ 5–$10\,\%$ for the heavier halogens which is slightly larger than the *s-d* mixing of $\sim 3\%$ for the rare-gas atoms [10(b)].

To obtain a full picture of the halogens we now examine the interaction between two channels which have outer *d* electrons but different *LS*-coupled target states. Specifically, we will study the $\underline{K}$ (reaction-reactance) matrix for the $^2P^e$ final-state symmetry. The general conclusions we draw for this symmetry also apply to the $^2D^e$ final-state symmetry. The $^2P^e$ symmetry contains three interacting channels: $ns^2np^4\,{}^3P\epsilon s$, $ns^2np^4\,{}^3P\epsilon d$, and $ns^2np^4\,{}^1D\epsilon d$. For the purpose of investigating the interaction between two ϵd channels we will completely ignore the rows and columns of the $\underline{K}$ matrix referring to the ϵs channel. Since the ϵs channel interacts weakly with the two ϵd channels, this deletion will not seriously affect our study of the qualitative *d-d* interaction dynamics. In the following paragraph, the $^3P\epsilon d$ and the $^1D\epsilon d$ channels will be called the ^3P and ^1D channels. Because we have reduced the $\underline{K}$ matrix to 2×2, we can again probe the dynamics through the study of a mixing angle θ and two quantum-defect eigenvalues μ_1 and μ_2.

In Fig. 13 we plot the dynamical parameters θ, μ, and $P_d d$ for the ^3P and ^1D channels. Again we see the striking similarity between the heavier halogens and their major difference from F. It is perhaps not clear from Fig. 13(b) that the quantum defects for F are both small, ~ 0.05 and ~ 0.0. Inserting these values into Eq. (10), we find that the probability for scattering from the ^3P into the ^1D channel (and vice versa) is $\sim 1\%$ [and in fact can hardly be seen in Fig. 13(c)]. This observation accounts for the very narrow ^1Dnd resonance in F, i.e., the electron must scatter from the core a large number of times before there is appreciable amplitude for finding it in the escape

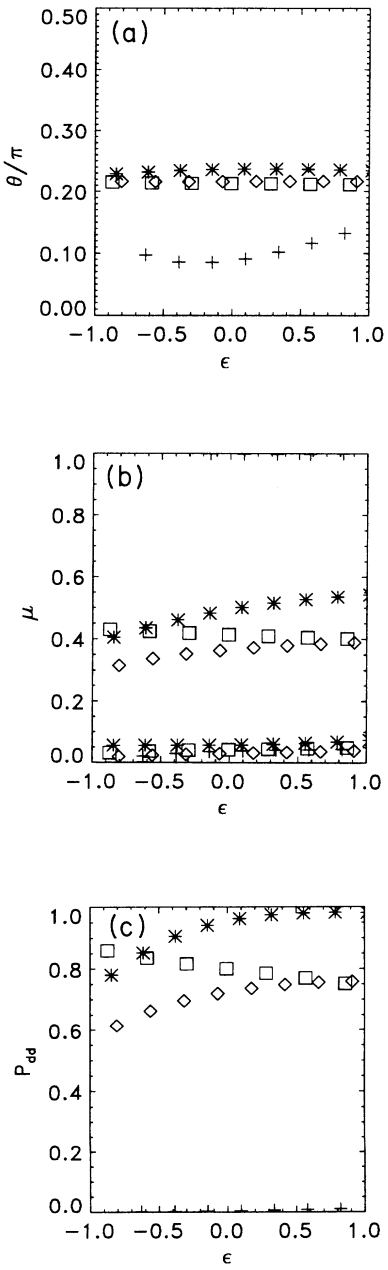

FIG. 13. Same as Fig. 12 except for the $^2P^e$ final-state symmetry with the $^3P\epsilon s$ channel removed.

channel. However, for the heavier halogens the dynamical parameters are such that maximal decay rates obtain. Figure 13(c) shows a probability of 60–100 % for scattering from the ^3P into the ^1D channel (and vice versa). For such a large probability the widths of the resonance becomes nearly equal to the spacing between the resonances.

The semiempirical determination of the Cl MQDT parameters in Ref. [35] is flawed by an error in the assignment of the broad resonances below the ^1D threshold to the $^2P^e$ final-state symmetry only. At that time these resonances were thought to be composed of only one Rydberg series whereas now we know them to be composed of two series of almost the same width with slightly different quantum defects and different final-state symmetries, $^2P^e$ and $^2D^e$. With the qualification we can compare the results of Ref. [35] for the mixing of what they call the $^3Pmd\,^2P^e$ and $^1Dmd\,^2P^e$ channels with our parameters plotted in Fig. 13. Their values of $\mu_1=0.31$, $\mu_2=0.09$, and $\theta=0.28\pi$ compare well with our values (near $\epsilon=-1$ where they did their fitting) of $\mu_1=0.4$, $\mu_2=0.05$, and $\theta=0.23\pi$. The operation $\theta\rightarrow\pi/2-\theta$ simply interchanges the labels on the eigenchannels and thus the experimental determination of the MQDT parameters for this final-state symmetry nearly reproduces our results even though they did not know the broad resonances are the sum of $^1Dmd\,^2P^e$ and $^1Dmd\,^2D^e$ autoionizing series. However, their fitted dipole matrix elements are quite different from our results which definitely stems from the error in their fitted number of channels.

VII. CONCLUSIONS

We have calculated the *LS*-coupled K matrices and dipole matrix elements necessary for the calculation of the photoionization of the halogens between their ns^2np^4 thresholds. We have analyzed these parameters to obtain more insight into the dynamics of these atoms and the good agreement between our calculated spectra and the experiments give us confidence in their accuracy. The similarity in the dynamics of the halogen atoms should be a trait common to other open-*p*-shell atoms (e.g., P, As, and Sb) and may help in the classification of their autoionization spectra. We have identified a dynamical frame transformation which will be necessary for a relativistic treatment of atoms with more than one hole or one electron in the outer shell in the target state. For Br and I, the discrepancy between theory and experiment may stem in part from the inadequate state of experimental knowledge of the energy levels of the charge 6+ ions which we need to determine the one-electron valence potentials.

ACKNOWLEDGMENTS

We thank J. Berkowitz for supplying us with magnified figures of his experimental data (Refs. [1–4]) and for suggestions and comments on this manuscript. We thank A. Robey for helping us with the Br VII and I VII references. This research is supported by the Division of Chemical Sciences, Office of Basic Energy Sciences, Office of Energy Research, U.S. Department of Energy Grant No. DE-FG-02-90ER14145.

[1] B. Ruščić, J. P. Greene, and J. Berkowitz, J. Phys. B **17**, L79 (1984).
[2] B. Ruščić and J. Berkowitz, Phys. Rev. Lett. **50**, 675 (1983).
[3] B. Ruščić, J. P. Greene, and J. Berkowitz, J. Phys. B **17**, 1503 (1984).
[4] J. Berkowitz, C. H. Batson, and G. L. Goodman, Phys. Rev. A **24**, 149 (1981).
[5] W. R. Fielder and L. Armstrong, Jr., Phys. Rev. A **28**, 218 (1983).
[6] E. R. Brown, S. L. Carter, and H. P. Kelly, Phys. Rev. A **21**, 1237 (1980).
[7] M. Lamoureux and F. Combet Farnoux, J. Phys. (Paris) **40**, 545 (1979).
[8] (a) S. Shahabi, A. F. Starace, and T. N. Chang, Phys. Rev. A **30**, 1819 (1984); (b) S. T. Manson, A. Msezane, A. F. Starace, and S. Shahabi, Phys. Rev. A **20**, 1005 (1979).
[9] A. F. Starace, in *Corpuscles and Radiation in Matter I*, edited by S. Flügge and W. Mehlhorn, Handbüch der Physik Vol. 31 (Springer-Verlag, Berlin, 1982).
[10] (a) C. M. Lee and K. T. Lu, Phys. Rev. A **8**, 1241 (1973); (b) C. H. Greene, J. Opt. Soc. Am. B **4**, 775 (1987).
[11] C. H. Greene, Phys. Rev. A **32**, 1880 (1985).
[12] P. G. Burke and W. D. Robb, Adv. At. Mol. Phys. **11**, 143 (1975).
[13] U. Fano and A. R. P. Rau, *Atomic Collisions and Spectra* (Academic, Orlando, 1986); M. J. Seaton, Rep. Prog. Phys. **46**, 167 (1983).
[14] C. H. Greene and M. Aymar, Phys. Rev. A **44**, 1773 (1991), and references therein.
[15] L. Kim and C. H. Greene, J. Phys. B **22**, L175 (1989).
[16] C. H. Greene and L. Kim, Phys. Rev. A **38**, 5953 (1988).
[17] W. Johnson, D. Kolb, and K.-N. Huang, At. Data Nucl. Data Tables **28**, 333 (1983).
[18] C. E. Moore, in *Atomic Energy Levels,* Natl. Bur. Stand. (U.S.) Circ. No. 467 (U.S. GPO, Washington, DC, 1949), Vol. I for the F VII and Cl VII energy levels.
[19] Y. N. Joshi and Th. A. M. Van Kleef, Can. J. Phys. **64**, 330 (1986).
[20] V. Kaufman and J. Sugar, Phys. Scr. **24**, 738 (1981).
[21] C. D. H. Chisholm and U. Öpik, Proc. Phys. Soc. London **83**, 541 (1964).
[22] (a) R. D. Cowan, *The Theory of Atomic Structure and Spectra* (University of California Press, Berkeley, 1981); (b) U. Fano, Phys. Rev. **140**, A67 (1965).
[23] P. O. Löwdin, Phys. Rev. **97**, 1474 (1955); P. O. Löwdin and H. Shull, *ibid.* **101**, 1730 (1956); C. Froese-Fischer, J. Comput. Phys. **13**, 502 (1973).
[24] R. E. Huffman, J. C. Larrabee, and Y. Tanaka, J. Chem. Phys. **47**, 856 (1967).
[25] (a) J. Berkowitz and G. L. Goodman, J. Chem. Phys. **71**, 1754 (1979); (b) J. Berkowitz and G. L. Goodman, J. Chem. Phys. **94**, 321 (1991).
[26] U. Fano, Phys. Rev. A **32**, 617 (1985).
[27] B. Ruščić and J. Berkowitz, Phys. Rev. A **40**, 6716 (1989).
[28] J. E. Hanson, R. D. Cowan, S. L. Carter, and H. P. Kelly, Phys. Rev. A **31**, 1515 (1985); V. F. Orlov, N. A. Cherepkov, and L. V. Chernysheva, Opt. Spektrosk. **64**, 683

(1988) [Opt. Spectrosc. (USSR) **64**, 409 (1988)].
[29] J. A. R. Samson, Y. Shefer, and G. C. Angel, Phys. Rev. Lett. **56**, 2020 (1986).
[30] N. A. Cherepkov and L. V. Chernysheva, Phys. Lett. **60A**, 103 (1977); Izv. Akad. Nauk SSR, Ser. Fiz. **41**, 2518 (1977) [Bull Acad. Sci. USSR, Phys. Ser. **41**, 47 (1977)]; V. G. Yarzhensky, V. I. Nefedov, M. Ya. Amusia, N. A. Cherepkov, and L. V. Chernysheva, J. Electron Spectrosc. Relat. Phenom. **23**, 175 (1981).
[31] F. Combet Farnoux and M. Ben Amar, J. Electron Spectrosc. Relat. Phenom. **41**, 67 (1986).
[32] P. van der Meulen, M. O. Krause, C. D. Caldwell, S. B. Whitfield, and C. A. de Lange, J. Phys. B **24**, L573 (1991).
[33] P. van der Meulen, M. O. Krause, and C. A. de Lange, J. Phys. B **25**, 97 (1992).
[34] H. G. Berry, L. P. Sommerville, L. Young, and W. J. Ray, J. Phys. B **17**, 3857 (1984).
[35] Z.-W. Wang and K. T. Lu, Phys. Rev. A **31**, 1515 (1985).